

# Computer Simulation of Constricted High Current Vacuum Arc Motion under Action of Transversal Magnetic Field<sup>1</sup>

D.L. Shmelev, T. Delachaux\*, and E. Schade\*

*Institute of Electrophysics, Ekaterinburg, 620016, Russia*

*Phone: +8(3432) 67-87-81, E-mail: Shmelev@iep.uran.ru*

*\*ABB Switzerland Ltd Corporate Research, Baden, 5405, Switzerland*

**Abstract** – The paper deals with the numerical simulation of the constricted high-current vacuum arc, driven by a transverse magnetic field (TMF). The 2D magnetohydrodynamic approach, radiative transfer in P1 approximations, together with the detailed heat transfer and evaporation equations for the electrodes, is used to describe the arc behavior self-consistently. The developed model describes the cathode attachment of the constricted arc, as a large laterally extended foot points, instead of regular cathode spots. This model leads to the characterization of the physical quantities of the arc plasma and describes the arc motion.

## 1. Introduction

The present paper focuses on the numerical modeling of constricted vacuum arcs driven by a transverse magnetic field (TMF), such as found in vacuum circuit breakers [1–3]. Such kind of moving arcs is used in vacuum circuit breakers, and in vacuum arc rail gun. In case of vacuum interrupters (spiral or cup-shape TMF contacts) arc motion distributes the heat flux from arc onto contacts. It improves interruption capability. Arc velocities range from several hundreds meters per second in case of interrupters up to several kilometers per second in case of rail gun. Arc current density estimated from experimental observations surpasses  $10^4$  A/cm<sup>2</sup>. The current density is high enough to heat the metal surface under the footpoints up to temperatures exceeding the evaporation temperature [2]. The metal vapor goes to the interelectrode gap, where vapor should be ionized to provide the conducting media for the arc operation. There are experimental observations that the evaporation looks as a two vapor jets originating from the footpoints and outflowing in the direction of arc motion [3].

## 2. Model description

The model describes the motion of the constricted arc in two-dimensional flat geometry (Fig. 1). The model consists of the following parts: interelectrode plasma – describes the plasma column behavior; anode and cathode attachment zones – describes the plasma – surface interaction, electron emission, and evapora-

tion; electrode part – calculates temperature of anode and cathode.

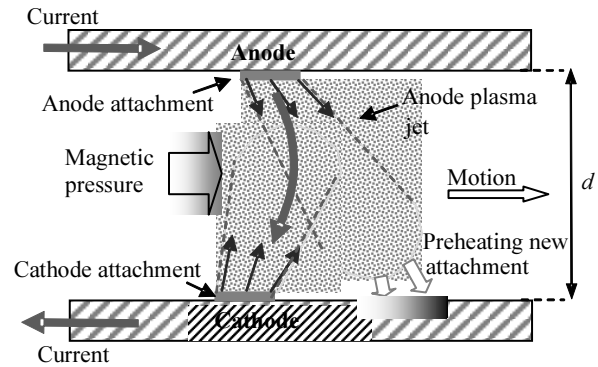


Fig. 1. Geometry of task and sketch of arc motion

Preliminary estimations based on 1D calculation showed that typical plasma density in the constricted arc should be on the order of  $10^{18}$  cm<sup>-3</sup> and temperature on the order of several electronvolts. These plasma conditions allow the application of the two-temperature MHD approach:

$$\frac{\partial n_k}{\partial t} + \text{div } n_k \vec{u} = \dot{n}_k, \quad k = 0, \dots, 3; \quad (1)$$

$$\dot{n}_k = (\alpha_{k-1} n_{k-1} - \beta_{k-1} n_k n_e - \alpha_k n_k + \beta_k n_{k+1} n) n_e;$$

$$m n \left( \frac{\partial \vec{u}}{\partial t} + \vec{u} \cdot \nabla \vec{u} \right) = -\nabla (n_e T_e + n T) + \frac{1}{c} [\vec{J} \times \vec{B}]; \quad (2)$$

$$\frac{3}{2} n \left( \frac{\partial T}{\partial t} + \vec{u} \cdot \nabla T \right) + n T \text{div } \vec{u} = 3 \frac{m_e}{m} \frac{n_e}{\tau} (T_e - T); \quad (3)$$

$$\frac{3}{2} n_e \left( \frac{\partial T_e}{\partial t} + \vec{u}_e \cdot \nabla T_e \right) + n_e T_e \text{div } \vec{u}_e + \text{div } \vec{Q}_e = \quad (4)$$

$$= 3 \frac{m_e}{m} \frac{n_e}{\tau} (T_e - T) + \frac{\vec{J}^2}{\sigma} + \frac{\beta}{e} \vec{J} \cdot \nabla T_e - E_{\text{ioniz}} - E_{\text{rad}};$$

$$\frac{\partial B_z}{\partial t} + \frac{\partial u_{e,y} B_z}{\partial y} + \frac{\partial u_{e,x} B_z}{\partial x} = \quad (5)$$

$$= \frac{c^2}{4\pi} \left( \frac{\partial}{\partial x} \frac{1}{\sigma} \frac{\partial B_z}{\partial x} + \frac{\partial}{\partial y} \frac{1}{\sigma} \frac{\partial B_z}{\partial y} \right);$$

<sup>1</sup> This work was partially supported by Russian Foundation for Basic Research (Grant Nos. 08-08-00801 and 08-02-00720).

$$\nabla \times \vec{B} = \frac{4\pi}{c} \vec{J}, \quad \vec{u}_e = \vec{u} - \frac{\vec{J}}{en_e}, \quad n_e = Zn. \quad (6)$$

The different parameters mean:  $n$  – density of heavy component (neutrals + ions);  $n_e$  – electron density;  $n_k$  – density of  $k$ th ion component;  $\alpha_k, \beta_k$  – ionization and recombination coefficient;  $u$  – heavy component drift velocity;  $u_e$  – electron drift velocity;  $T$  – heavy component temperature;  $T_e$  – electron temperature;  $J$  – arc current density;  $Z$  – average charge state of ions;  $\tau$  – electron-ion collision time;  $Q_e$  – electron thermal flux;  $E_{rad}$  – energy loss by radiation;  $E_{ioniz}$  – energy loss due to ionization – recombination processes;  $\beta$  and  $\gamma$  – Braginskii coefficients;  $\sigma$  – conductivity;  $B$  – magnetic field. Only  $z$ -component of magnetic field  $B_z$  exists in the present model. Explicit expression for the mentioned coefficients and detailed description of the equation set can be found in [4].

The radiation energy loss  $E_{rad}$  in equation (4) in the previous work [5] was calculated with help of net emission coefficient approximation. The calculations showed that the term is very significant and, therefore, the more sophisticated method needs to be used. The P1 method [6] was chosen as a compromise between efficiency and accuracy. The method reduces the radiative transport equation to the system of Helmholtz-type equations

$$\nabla \cdot \left( \frac{1}{k_v} \nabla G_v \right) = 3k_v (G_v - 4\pi I_{bv}), \quad (7)$$

where  $G_v$  – incident radiation;  $k_v$  – absorption coefficient;  $I_{bv}$  – black body radiation intensity. The spectrum of absorption coefficient was divided into seven bands. Then it's necessary to solve only seven equations (7) – one for each band, and the total radiation energy loss can be obtained as follows:

$$E_{rad} = \sum_{v=1}^7 \bar{k}_v (4\pi \bar{I}_{bv} - \bar{G}_v), \quad (8)$$

where dash above the letters means integration (averaging in case of  $k$ ) over the  $v$ th band.

Attachment zone of constricted arc looks like a solid bright region. They are no experimental evidence that this bright region consists of small cathode spots. An assumption was made that the attachment zone of constricted arc behaves like one “big cathode spot”. Average current density in such big spot is about  $10^4 \div 10^5$  A/cm<sup>2</sup> [2] that considerably less then current density  $10^7 \div 10^9$  A/cm<sup>2</sup> estimated for the “conventional” small cathode spots. Considerable number of different models was developed to describe cathode spot physics [7]. An approach developed in the theories of nonexplosive quasi-stationary type was chosen to construct the comparatively simple model of cathode attachment.

Thickness of attachment zone is on the order of several mean free path length. This length is much less

then interelectrode gap distance. Because of it, a local 1D approach was used for attachment model.

Richardson–Schottky equation was used to calculate emission electron current density  $J_{em}$ :

$$J_{em} = 120T_{cs}^2 \exp\left(-\frac{\phi'}{T_{cs}}\right); \quad \phi' = \phi - \sqrt{e^3 E_c}, \quad (9)$$

where  $T_{cs}$  – cathode surface temperature, cathode electric field  $E_c$  is obtained from Mackeown equation:

$$E_c^2 = 16\pi \sqrt{\frac{m_e U_c}{2e}} \left( J_i \sqrt{\frac{m_i}{m_e}} - J_{em} \right), \quad (10)$$

where cathode drop voltage  $U_c$  is taken from

$$U_c = (J_i I_1 - J_{em} 2T_{cs}) / J_{em} + U_0, \quad (11)$$

where  $I_1$  is the first ionization potential. Equation (11) means that energy going to plasma with emission electrons must be enough to provide all necessary ion current plus some energy  $U_0$ , which going further to plasma column. Parameter  $U_0$  is a task parameter. It is chosen to be 5 V in the present calculation. Ion current density is obtained from:

$$J_i = J - J_{em}. \quad (12)$$

Equations (9)–(12) are iterated for each point of cathode attachment zone for given  $T_{cs}$  and  $J$ . Distribution of total current density  $J$  along the attachment zone is calculated from solution of equation (5) with the following cathode boundary condition:

$$E_x \equiv \frac{J_x}{\sigma} - \frac{1}{c} u_{e,y} B - \frac{1}{en_e} \frac{\partial n_e T_e}{\partial x} = -\frac{\partial U_c}{\partial x}. \quad (13)$$

Equation (13) arises from condition of the nullifying of Hall field in the plasma close to electrode surface.

Attachment zone is also a source of material for plasma column. Flux of evaporated atom is obtained from [8]:

$$G_{cv} = \frac{2P_s}{\sqrt{2\pi m T_s}} \left( 1 - \frac{nT + mnu^2}{P_s} \right), \quad (14)$$

where  $P_s$  is saturation pressure. Then the net flux from cathode to plasma is

$$G_{ctot} = G_{cv} - J_i / e. \quad (15)$$

The anode side of high current vacuum arc also has a mechanism, which leads to the constriction of current and appearing of bright anode spot. This spot like the cathode one also provides the source of material for plasma column. It is assumed that anode connection of the modeling arc corresponds to the anode spot.

Distribution of total current density along the anode attachment area is obtained from solution of equation (5) with the following boundary conditions:

$$E_x \equiv \frac{J_x}{\sigma} - \frac{1}{c} u_{e,y} B - \frac{1}{en_e} \frac{\partial n_e T_e}{\partial x} = -\frac{\partial U_a}{\partial x}, \quad (16)$$

where  $U_a$  is the anode voltage drop. Equation (16) has the same sense like (13), but the voltage drop is calculated from the following system:

$$U_a = \frac{T_e}{e} \ln \left( \frac{J + J_i + J_{em}}{J_{th}} \right); \quad J_{th} = en_e \sqrt{\frac{T_e}{2\pi m_e}}, \quad (17)$$

where  $J_{th}$  – electron thermal current from plasma;  $J_{em}$  – emission electron current from anode to plasma, which calculated from Richardson–Schottky equation (9) together with the generalized form of Mackeown equation including thermal current from plasma;  $J_{ai}$  – ion current from plasma to the anode obtained as follows:

$$J_{ai} = e z n \cdot \max \left( 0.61 \sqrt{(T_i + z T_e)/m_i}, u_i \right). \quad (18)$$

Evaporation from the anode attachment zone is obtained from the equation similar to (14), (15).

To obtain the electrodes surface temperature, the 2D thermal conductivity equation in the electrodes was solved. Only surface heating by action of thermal flux from plasma and thermal conductivity was taken into account. Effects linked with joule heating and surface motion were neglected.

Place and extension of attachment zones are determined from surface temperature distribution. Cathode attachment zone must provide enough thermionic current and vapor flux to sustain the arc operation. Calculations showed that in case of copper electrode, this condition is fulfilled then the cathode surface temperature exceeds 3400 K. Temperature threshold value for the anode attachment zone is 2900 K. The anode attachment area must have high temperature to provide enough plasma density in order to avoid positive voltage drop. Threshold temperatures are well above the boiling temperature (for Cu – 2840 K). Temperature within the attachment zones is higher and can reach 4000 K. There is no direct experimental proof of the high surface temperatures predicted by the numerical simulation. However, authors [2] have estimated the electrode temperature at the foot points of a TMF constricted arc, at anode between 3300 and 3600 K and at cathode between 3200 and 3400 K, respectively. Their results support the assumption of the present model.

### 3. Numerical results and discussion

Schematically, the work of the computer program based on the model described above looks as follows. The simulations are started assuming an initial condition with a homogenous plasma column having temperatures of 2 eV and plasma density of  $10^{18} \text{ cm}^{-3}$ . Initial conditions for attachment zones correspond to the position and size of the column. It is necessary to tell

that the chosen initial condition does not influence the rest of the calculations. The arc forgets it after several microseconds. After the external TMF is switched on, the column under action of magnetic pressure starts to bend to the right direction (Fig. 1). Thermal flux from plasma column heats the electrode surface. When the surface temperature reaches the threshold value, a new attachment zone arises at this position. In addition, when the surface temperature within the attachment zone falls below the threshold value, the attachment is switched off at this point. Thus, the arc moves to the right side.

The arc plasma column is formed by two opposite jets originated from the electrode attachment zones. Plasma in the column is fully ionized. Pressure of plasma reaches several tens bar (Fig. 2).

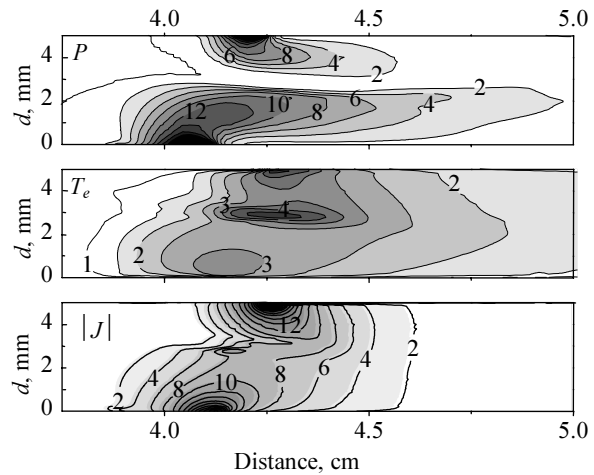


Fig. 2. Plasma pressure  $P$ , Bar; electron temperature  $T_e$ , eV; current density  $|J|$ ,  $10^4 \text{ A/cm}^2$ ; at time  $60 \mu\text{s}$ .  $B_{\text{ext}} = 1 \text{ T}$ ,  $I = 30 \text{ kA}$

Pressure usually has maximum values nearby the electrode attachment zones, where the pressure is close to saturated pressure, which corresponds to the surface temperature. Electron temperature has the typical value in the middle of column about  $2\div 3 \text{ eV}$  (Fig. 2). Ion temperature is usually close to electron one within the column. Ion temperature can deviate from electron temperature close the attachment zones, where the strong evaporation and ionization processes are happening. In addition, ion temperature usually exceeds the electron one in the area of two opposite jet interaction, where a strong shock wave can exist.

Plasma inside the jets is accelerated by action both gasodynamic pressure and magnetic pressure. Because of asymmetric of the magnetic field, the jets are bended to the right side. Plasma drift velocities of the order of  $10^6 \text{ cm/s}$  are obtained in the center gap region. The parameters distributions on anode and cathode are different (Fig. 3). Current at the anode side is more constricted. This result to the following: size of anode attachment is smaller; maximum of energy flux to the electrode is higher; maximum of surface temperature is also higher. All of these, in turn, lead to the

fact that the anode attachment drift speed is higher than the cathode one at the conditions being equal.

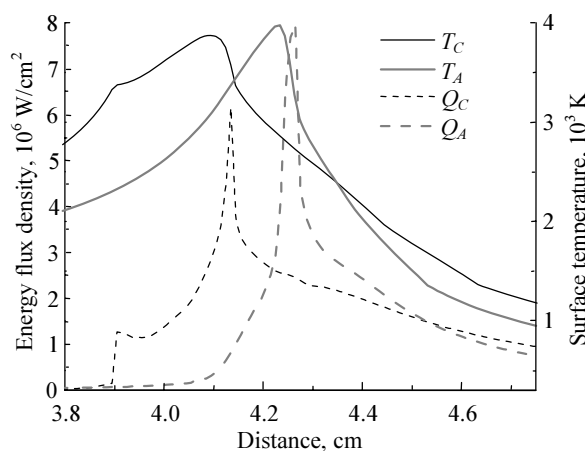


Fig. 3. Surface temperatures  $T_C$ ,  $T_A$ , energy flux densities  $Q_C$ ,  $Q_A$  on cathode end anode correspondently. Time – 60  $\mu$ s.  $B_{ext} = 1$  T,  $I = 30$  kA

Calculation showed that the motion of modeled arc has two modes: the slow continuous drift of attachment zones and a step-wise motion then the new connection area appears at certain distance from the old one. Drift mode exists at the low external TMF. New attachment points are preheated in immediate vicinity to the old ones and the zone shifting continuously. The anode connection is always ahead of cathode connection in this mode. Arc looks roughly like an inclined column (Fig. 2). Angle of this inclination is approximately conserved during motion. Some oscillations of plasma column exist but the arc in whole keeps stability and self-similarity. Magnetic pressure and momentum of anode jet is balanced by momentum of cathode jet. The angle of column inclination grows with external TMF increasing. At certain critical value of the angle, the arc loses stability. Cathode jet cannot more balance the action of anode jet and magnetic force. Plasma of anode jet strikes the cathode surface. As a result, the new attachment zone appears at certain distance from the old one. Thus, the arc makes a step. Now, the cathode connection is ahead of the anode one and a similar sequence will happen. Picture series in Fig. 4 shows the described step-wise motion.

Figure 5 shows the displacement of the front edge of the anode and cathode connection versus time at the different values of external TMF.

When the field is low, only drift motion is exist and displacement line is smooth. The arc motion speed grows with the field but slowly. At the value 1.2 T the step-wise motion appears. Displacement line contains now a number of plateaus, which are the parts of the drift motion between the steps. The rate of the arc speed growing with TMF value increases considerably with step-wise mode appearing. The following increasing of speed happens mainly due to reduction of the time, when the arc stays in the drift mode.

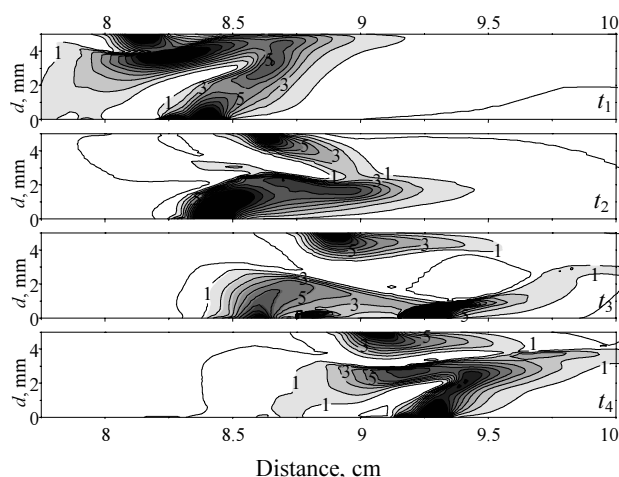


Fig. 4. Plasma pressures (bar) at time steps:  $t_1 = 80$   $\mu$ s,  $t_2 = 83$   $\mu$ s,  $t_3 = 86$   $\mu$ s,  $t_4 = 87$   $\mu$ s;  $B_{ext} = 1.2$  T;  $I = 30$  kA

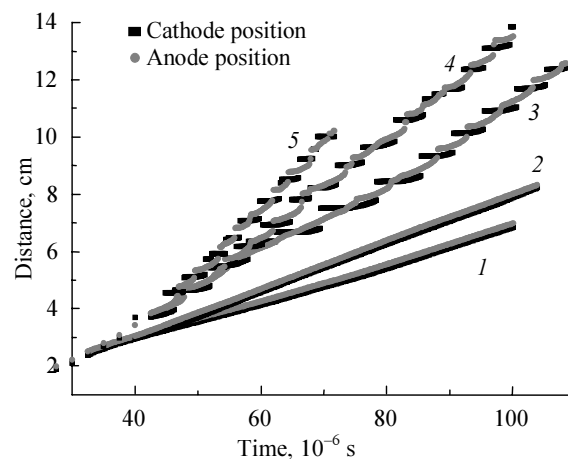


Fig. 5. Attachment displacement vs time;  $d = 0.5$  cm,  $I = 30$  kA: 1 –  $B_{ext} = 1$  T,  $V_{arc} = 650$  m/s; 2 –  $B_{ext} = 1.1$  T,  $V_{arc} = 830$  m/s; 3 –  $B_{ext} = 1.2$  T,  $V_{arc} = 1280$  m/s; 4 –  $B_{ext} = 1.3$  T,  $V_{arc} = 1670$  m/s; 5 –  $B_{ext} = 1.4$  T,  $V_{arc} = 2200$  m/s

Figure 5 shows that the arc moves with the approximately constant average speed ( $V_{arc}$ ) after several tens microseconds. This  $V_{arc}$  was calculated from Fig. 5 by the linear fitting. For present conditions the speed varies from six hundreds up to two thousands meters per second. The last value is more suitable for the vacuum arc rail gun. There is nothing strange in it. Indeed, the present electrode system is rather the rail gun than the vacuum interrupter. Thus, in the particular case it can be one of the possible validations of the model. Arc speed in interrupter is measured on the level of several hundreds meters per second, that also doesn't conflict with the model.

## References

- [1] E. Dullni, IEEE Trans. Plasma Sci. **17**, No. 6, 875–879 (1989).
- [2] W. Haas and W. Hartmann, IEEE Trans. Plasma Sci. **27**, 954–960 (1999).

- [3] E. Dullni, E. Schade, and W. Shang, *IEEE Trans. Plasma Sci.* **31**, No. 5, 902–908 (2003).
- [4] S.I. Braginskii, *Reviews of plasma physics* / M.A. Leontovich, ed., New York, Consult. Bureau, 1965.
- [5] T. Delachaux, O. Fritz, D. Gentsch, E. Schade, and D.L. Shmelev, *IEEE Trans. Plasma Sci.* **35**, 905–911 (2007).
- [6] S.D. Eby, J.Y. Trepanier, and X.D. Zhang, *J. Phys. D. Appl. Phys.* **31**, 1578–1588 (1998).
- [7] I.I. Beilis, *IEEE Trans. Plasma Sci.* **29**, 657–670 (2001).
- [8] V.I. Mazhukin and A.A. Samohkin, *Matematicheskoe modelirovanie*, Moscow, Nauka, 1987, pp. 191–244 [in Russian].